

Articles

Antiproliferative and Phenotype-Transforming Antitumor Agents Derived from Cysteine

Matthew P. Glenn,[†] Pia Kahnberg,[†] Glen M. Boyle,[‡] Karl A. Hansford,[†] Dhiraj Hans,[†] Adam C. Martyn,[‡] Peter G. Parsons,[‡] and David P. Fairlie*[†]

Centre for Drug Design and Development, Institute for Molecular Bioscience, University of Queensland, Brisbane, Queensland 4072, Australia, and Melanoma Genomics Group, The Queensland Institute for Medical Research, Herston, Queensland 4006, Australia

Received May 13, 2003

Selective destruction of malignant tumor cells without damaging normal cells is an important goal for cancer chemotherapy in the 21st century. Differentiating agents that transform cancer cells to either a nonproliferating or normal phenotype could potentially be tissue-specific and avoid side effects of current drugs. However, most compounds that are presently known to differentiate cancer cells are histone deacetylase inhibitors that are of low potency or suffer from low bioavailability, rapid metabolism, reversible differentiation, and nonselectivity for cancer cells over normal cells. Here we describe 36 nonpeptidic compounds derived from a simple cysteine scaffold, fused at the C-terminus to benzylamine, at the N-terminus to a small library of carboxylic acids, and at the S-terminus to 4-butanoyl hydroxamate. Six compounds were cytotoxic at nanomolar concentrations against a particularly aggressive human melanoma cell line (MM96L), four compounds showed selectivities of $\geq 5:1$ for human melanoma over normal human cells (NFF), and four of the most potent compounds were further tested and found to be cytotoxic for six other human cancer cell lines (melanomas SK-MEL-28, DO4; prostate DU145; breast MCF-7; ovarian JAM, CI80–13S). The most active compounds typically caused hyperacetylation of histones, induced p21 expression, and reverted phenotype of surviving tumor cells to a normal morphology. Only one compound was given orally at 5 mg/kg to healthy rats to look for bioavailability, and it showed reasonably high levels in plasma (C_{\max} 6 $\mu\text{g/mL}$, T_{\max} 15 min) for at least 4 h. Results are sufficiently promising to support further work on refining this and related classes of compounds to an orally active, more tumor-selective, antitumor drug.

Introduction

Current antitumor agents are general cytotoxins, nonselectively killing normal as well as tumor cells, leading to side effects. Truly selective cancer chemotherapy in which a drug specifically destroys malignant tumor cells without damaging normal cells remains an elusive goal in the 21st century. One promising strategy^{1–4} is the use of agents that can differentiate cancer cells to either a nonproliferating or normal phenotype, an approach that has the potential to be tissue-specific and avoid side effects of current drugs. Most compounds known to differentiate tumor cells are of low potency in cell culture (e.g. $\text{IC}_{50} > 1 \mu\text{M}$; butyrate, retinoic acid, HMBA, ABHA, SBHA, SAHA, scriptaid, and sirtinol^{5–9}) and tend to be nonselective in vivo, where differentiation is reversible or drug resistance is a problem. Nevertheless, such compounds have shown promising antitumor properties in vivo, suggesting that more potent differentiating agents should be studied. A few natural products (e.g. trichostatin,^{10,11} trapoxin,¹² apicidin¹³) and close analogues^{14–18} display more potent differentiating properties on cancer cells in vitro, but they are cytotoxic

to both normal and cancer cells and are ineffective in vivo due to low bioavailability and rapid metabolism.

All of the above differentiating agents are now known to cause hyperacetylation of histones, by inhibiting enzymes known as histone deacetylases (HDACs). It is also clear that multiprotein complexes incorporating HDACs are involved in cell cycle regulation and gene expression, HDACs modulating chromatin structure by facilitating unpackaging of chromosomal DNA, and 'loosening up' histones to permit transcription.¹⁹ Histones of the nucleosome are normally tightly wrapped in DNA and linked together like a string of beads by DNA. Nuclease-mediated digestion of both the linking and wrapping DNA from histones enables gene expression. Unwrapping exposes the octameric histone core, which dissociates into component histones H2A, H2B, H3, H4, etc.²⁰ Histones are reversibly acetylated on the ϵ -amino side chain of Lys residues (Figure 1), and interactions between *deacetylated* histones and DNA are crucial for gene expression. Histone acetylation and other modifications regulate gene expression by reducing access of transcription factors to DNA.^{12,21} The degree of histone acetylation is regulated by histone acetyl transferases (HATs; 3 groups), deacetylases (HDACs, 16 genes),^{5,20,22} and their inhibitors which

* Corresponding author. E-mail: d.fairlie@imb.uq.edu.au.

[†] University of Queensland, Brisbane.

[‡] The Queensland Institute for Medical Research.

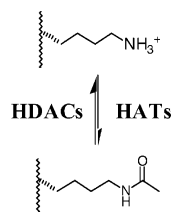
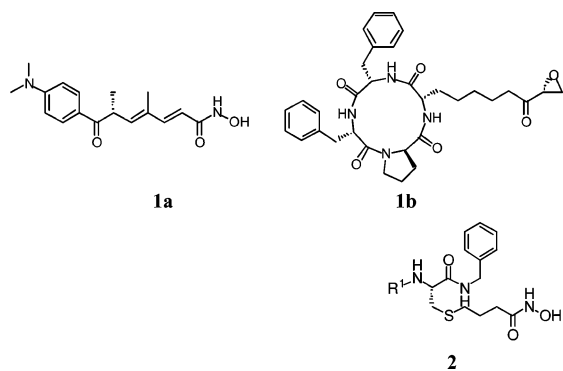


Figure 1. Acetylation/deacetylation of histone lysine side chains.

regulate the cell cycle and consequently hold promise for development of anticancer drugs. Studies by us and others indicate that HDAC inhibitors cause tumor regression in vivo without damaging DNA.^{20,22}

At least eleven HDACs have been identified^{23,24} and, although it is unknown to what extent these enzymes exercise redundant or specific functions, subtle sequence differences between HDACs suggest that it may be possible to develop specific inhibitors for specific HDAC enzymes. Crystallographic studies on the histone deacetylase-like protein (HDLP) isolated from *Aquifex aeolicus* indicate that the active site residues of these enzymes are highly conserved, with more variability at the entrance to this cleft, particularly on the solvent exposed rim of the active site that accommodates the lysine side chain. Furumai et al. have shown that a carboxylic acid analogue of trapoxin, which is a poor zinc ligand, is still potent with IC₅₀ of 100 nM probably due to making significant interactions with the surface at the entrance to the HDAC active site.¹⁵

Herein we describe a facile entry to new antitumor compounds, designed to reproduce and modify protein surface-binding interactions made by hydrophobic substituents found in highly potent naturally occurring HDAC inhibitors, such as trichostatin (**1a**) and the cyclic tetrapeptides trapoxin B (**1b**) and apicidin. Acyclic compounds specifically based on structure **2** below,



composed of a simple cysteine scaffold fused at the C-terminus to benzylamine, at the S-terminus to 4-butanoylhydroxamate, and at the N-terminus to a small library of carboxylic acids, display structural and bioactivity features characteristic of known HDAC inhibitors such as trichostatin **1a** and trapoxin **1b**. This small library explores relationships between structure and antitumor activity, particularly the influences of surface interactions adjacent to the active site entrance of HDACs. Since protein acetylation/deacetylation now appears to be a general cell signaling device, with many possible protein/DNA targets for HDAC inhibitors, we have used toxicity/selectivity for tumor cells as our

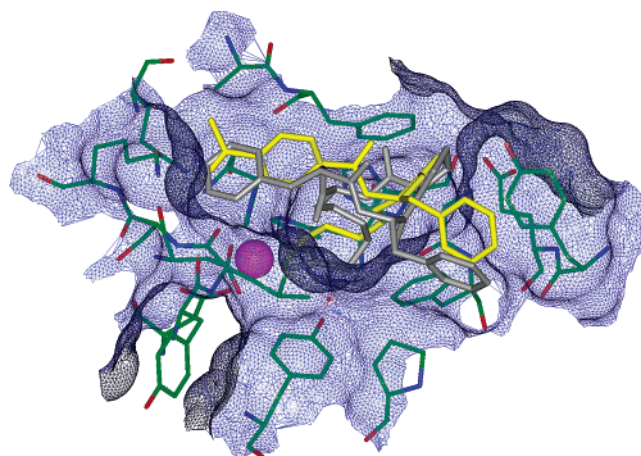


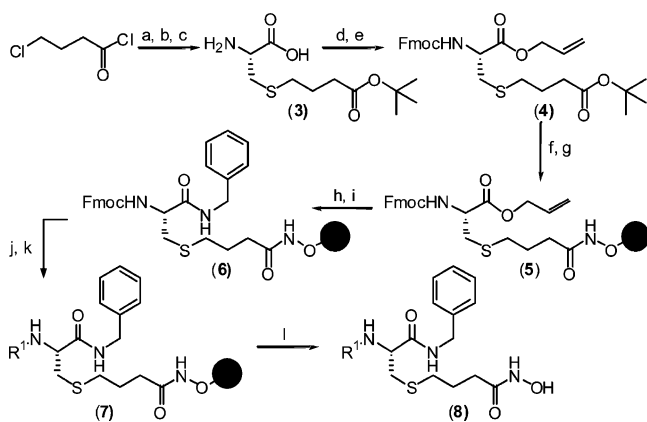
Figure 2. HDAC-binding inhibitor conformations. Comparison of the GOLD docked conformations of **1b** (grey) and **9** (yellow) in the active site of histone deacetylase from *Aquifex aeolicus* (blue, Zn ion pink). Shown in blue is the solvent accessible surface area and in green are protein residues within 3.0 Å of the inhibitor.

primary screen to guide our compound development, rather than directly measuring inhibition of specific HDACs. We still however monitor histone hyperacetylation caused by the more potent/selective drugs to verify HDAC activity. Because HDAC inhibition does correlate with potency of our compounds, if not selectivity, a general HDAC-inhibitor pharmacophore has been used to guide our design of drugs. However, our ultimate aim is to obtain enhanced cytoselectivity for tumor cells over normal cells, and this appears to be independent of HDAC potency.

Results and Discussion

Compound Design. The three-dimensional structure of HDLP has been solved both as the native enzyme and cocrystallized with the HDAC inhibitors **1a** (1c3r.pdb) and suberoylanilide hydroxamic acid (SAHA). HDLP shares ~32% homology with HDAC1 and deacetylates histones in vitro. High sequence homology is observed within the hydrophobic tubular catalytic active site, ~11 Å deep but narrowing to ~4 Å at the active site and terminating at a divalent zinc cation, activated water molecule, and histidine-aspartate charge-relay system.²⁵ Most of the residues in the HDLP structure that interact directly with **1a** are highly conserved among all the HDACs, but there is less conservation in adjoining residues, most notably on the enzyme surface which has a number of shallow pockets surrounding the active site channel.^{23,26}

Docking of **1b** into the HDLP crystal structure using a combination of conformational searching (MACRO-MODEL) and a genetic docking algorithm (GOLD) identified tight binding conformations in which the aliphatic side chain had inserted into the tubular pocket of the active site, with the Phe side chains in contact with the shallow pockets of the enzyme surface (Figure 2). These aromatic groups represent important foliage on the cyclic tetrapeptide scaffold for tight enzyme binding, and similar groups are represented in related naturally occurring cyclic tetrapeptides (Phe, Trp, Tyr). However, cyclic tetrapeptides offer limited scope for potential therapeutics due to their difficulty of synthe-

Scheme 1^a

^a (a) ^tBuOH, pyridine; (b) NaI, THF; (c) Cys, NaOH, MeOH; (d) Fmoc-OSu, NaHCO₃, THF, water; (e) allyl bromide, DMF, K₂CO₃; (f) TFA; (g) HATU, DIPEA, 2-chlorotriethylhydroxylamine resin, DMF; (h) Pd(PPh₃)₄, DMBA; (i) benzylamine, HBTU, DIPEA, DMF; (j) piperidine; (k) R¹-Acid, HBTU, DIPEA, DMF; (l) TFA.

sis, problematic stability, and conformational homogeneity. We aimed to reproduce the key enzyme binding regions of **1b**, which would include a zinc chelator tethered to a branched capping group capable of reproducing the approximate positions and orientations of the Phe side chains, on a much simplified template. It was envisaged that a tripeptide incorporating similar surface binding groups to those found in the potent naturally occurring cyclic tetrapeptide inhibitors (hydrophobic, aromatic, basic) would be able to span the surface binding domain of Trapoxin B, while a hydrophobic tether terminating at a hydroxamic acid would ensure tight zinc binding in the catalytic core.

L-Cysteine was selected as the ideal core building block for these hybrid inhibitors, as it provides a convenient source of asymmetry and can be appended to in three directions. The longer carbon–sulfur bond lengths, as compared to carbon–carbon bonds, provide a tether of intermediate length between the five to six methylene units thought to be optimal from studies of analogues of SBHA and ABHA. Additionally, the high polarization of sulfur improves water solubility, but does not unacceptably compromise the hydrophobic nature of the aliphatic tether. Thirty-six diversity elements were selected for the N-terminal side R¹ of **2**, while maintaining the C-terminal surface binding element. N-Terminal diversity included mono- and bicyclic, fused and unfused aromatic, heterocyclic, and aliphatic residues. The lipophilicity of the hydroxamic acids was calculated at pH 7 (Log *D*_{7.0} being the octanol/water partition coefficient) using PALLAS, with 23 compounds having Log *D* 1–3, 11 with Log *D* 0–1, and two compounds with Log *D* 3–4, in anticipation of suitable penetration of cell membranes.

Synthesis. Unprotected cysteine was alkylated at the nucleophilic sulfur with 4-iodobutyric acid *tert*-butyl ester (Scheme 1) to give amino acid **3**, with a side chain acid of suitable length to span the 11 Å tubular pocket of the active site of HDACs. Complete alkylation was observed within several minutes after addition of the iodide to L-cysteine in basic deoxygenated methanol. Under these conditions, no disulfide bond formation or amine alkylation were observed. Protection of the amine

as the fluorenylmethoxycarbamate and conversion of the free acid to an allyl ester provided orthogonally protected amino acid **4**.

Removal of the *tert*-butyl ester group of **4** with TFA resulted in the acid, which was coupled to the 2-chlorotriethylhydroxylamine resin in good yield (1 h, 70%) using HATU, which is more efficient than alternative coupling reagents such as HBTU or BOP. After fixing to the resin, the allyl ester was removed by treatment with Pd(0) in the presence of an allyl scavenger (DMBA), and the free acid was coupled to benzylamine. Deprotection of the N-terminal amine permitted coupling in parallel to a small library of 37 acids, giving inhibitors **9–45** in >80% purity after cleavage from resin. All inhibitors were purified to better than 95% purity by reversed phase HPLC.

Antiproliferative Activity against MM96L Melanoma Cells. The cytotoxicities of hydroxamic acids **9–45** were determined by clonogenic survival of human cancer cells (MM96L, melanoma) and human normal cells (NFF, neonatal foreskin fibroblasts). Cells were incubated with **9–45** at various concentrations of hydroxamic acid (0.01–10 μg/mL) for 24 h, washed, and then grown for a further 4 days in the absence of hydroxamic acid before determining cell survival by cell count. The final readout involved staining with sulforhodamine B (SRB), a cost-effective method amenable to automation and high throughput analysis. At the technical level, “cell sensitivity” is often inferred from short term (1–2 day) observations such as apoptosis, which may not be a satisfactory model of clonogenic survival. Compounds were considered for further testing if they exhibited either potency (IC₅₀ ≤ 200 nM) or selectivity (SI > 5) in their killing of cancer cells over normal cells.

Six of the thirty-seven compounds tested displayed an IC₅₀ < 1 μM (**9**, **11**, **12**, **25**, **27**, **35**) against MM96L cells, and four had IC₅₀ ≤ 200 nM (**9**, **11**, **27**, **35**), comparable in potency to TSA (IC₅₀ 30 nM) for this cell line under test conditions (Tables 1–3). The most potent cytotoxins possessed rigid elements of diverse structure at R¹. Para-substituted aromatic derivatives such as 4-(dimethylamino)- (**9**) and 4-bromo- (**11**), but not 4-fluoro- (**16**), benzoic acids were the more potent, as is *trans*-cinnamic acid (**35**) and the 2-carboxylindole analogue **27** (IC₅₀ MM96L 130–200 nM). The large para substituent in **12** (4-phenyl) had substantially reduced potency (IC₅₀ MM96L 900 nM) and identifies the limit of substitution that can be accommodated at this position. Ortho or meta substitution (**13–15**, **17–19**, **24–26**) resulted in low potency (IC₅₀ MM96L > 1 μM) in all cases.

Incorporation of flexible alkyl substituents (**36**, **37**) significantly reduced potency (IC₅₀ MM96L ~5 μM), as indicated by comparing active **12** and **35** with less active **33**, **34**, and **36**, where the 4-phenylbenzoic and *trans*-cinnamic acid units have been replaced by more flexible 3- and 4-phenylalkanoic acid derivatives. A similar loss of potency was observed for the benzyl derivatives **28–32**, where insertion of a single methylene unit prevents the fragment from projecting linearly from the amide bond. Other aliphatic, cyclic, and aromatic heterocyclic fragments provided limited cytotoxicity, as did sulfonamide derivatives.

Table 1. Structure–Activity Relationships for Analogues of **2**

Compound	R ¹	Log D _{7.0}	IC ₅₀ NFF (μM) ^a	IC ₅₀ MM96L (μM) ^b	Selectivity ^c
1a			0.20 ± 0.04	0.03 ± 0.01	6.7
9		2.1	0.35 ± 0.07	0.14 ± 0.09	2.5
10		0.0	>100	>100	
11		2.7	0.83 ± 0.09	0.2 ± 0.1	4.2
12		3.5	2.8 ± 0.2	0.9 ± 0.1	3.1
13		2.8	10.9 ± 0.9	2.0 ± 0.4	5.5
14		3.0	30 ± 1	24 ± 3	1.3
15		2.2	>100	28 ± 3	
16		1.5	26 ± 1	5.2 ± 0.6	5.0
17		1.5	4.5 ± 0.6	1.7 ± 0.3	2.6
18		0.7	4.5 ± 0.6	32 ± 3	0.14
19		0.9	>100	10.6 ± 0.1	

^a NFF, neonatal foreskin fibroblasts. ^b MM96L, melanoma cells. ^c Ratio of IC₅₀s.

These structure–activity relationships are consistent with the variable R¹ substituent occupying a narrow receptor pocket with a preference for rigid aromatic fragments. It is unclear whether aromatic heterocyclic fragments could be accommodated, because the low lipophilicity of these compounds (**22**, **23**) may have adversely affected cell penetration, although the secondary amine of **27** (versus analogue **35**) did not reduce activity. However the similar potencies of **27** and **35** suggest that hydrogen bonding or other stabilizing interactions between this amine and the enzyme have not been accessed.

Cytoselectivity. The MM96L melanoma and NFF normal cell lines selected above have well-established responses to HDAC inhibitors, which trigger G₁ and G₂ phase cell cycle arrest in NFF, but not in MM96L cells.²⁷ It is likely that altered expression of specific genes is critical to this selectivity. For example, the cyclin-dependent kinase (cdk) inhibitor p21^{WAF1/Cip1} has been consistently found to be induced in NFF, but not in MM96L cells. Inhibition of cdk leads to hypophosphorylation of retinoblastoma protein and subsequent transient G₁ phase arrest, providing protection against the cytotoxic effects of HDAC inhibition. MM96L cells lack this prophylactic phase arrest and enter apoptosis at lower doses than those required to cause cell death in normal functioning cells. However, compounds **9–45**

were only moderately selective (≤7-fold) in their cell killing properties for MM96L cells over NFF cells and no more selective than trichostatin. The selectivity index probably though underestimates the degree of cytoselectivity because, in many cases, less than 50% of normal cells die due to cell cycle arrest.

The four most active compounds (**9**, **11**, **27**, **35**) were also tested for cytotoxicity and cytoselectivity against six other human cancer cell lines (Table 4), two melanoma (SK-MEL-28, DO4), one prostate (DU145), one breast (MCF-7), and two ovarian (JAM, CI-80–13S). For comparison, the results are also shown for MM96L and NFF cell lines. Compound **27** showed the highest activity for all the cancer cell lines, five of the seven lines being inhibited at sub-micromolar concentrations, followed by **9** (four cancer cell lines), **35** (three), and **11** (one). All four compounds more effectively killed MM96L melanoma cells than the other six cancer cell lines. None of the compounds was more cytotoxic than the TSA, which also killed normal neonatal fibroblast cells more effectively (IC₅₀ 0.2 μM) than the test compounds.

The origin of the small differences in structure–selectivity relationships observed in Tables 1–4 is not yet clear, but may reflect the extent of inhibitor optimization for another specific cellular target(s) that ultimately differentially affects the onset of cell death. While the variable fragments R¹ chosen here to initially

Table 2. Structure–Activity Relationships for Analogues of **2**

Compound	R ¹	Log D _{7.0}	IC ₅₀ NFF (μM) ^a	IC ₅₀ MM96L (μM) ^b	Selectivity ^c
20		1.8	9 ± 1	2.5 ± 0.2	3.6
21		0.5	22 ± 1	7.2 ± 0.2	3.1
22		0.4	62 ± 5	19 ± 2	3.3
23		0.1	>100	12.8 ± 0.8	
24		2.8	5.3 ± 0.6	6.3 ± 0.6	0.8
25		2.8	1.14 ± 0.05	0.6 ± 0.2	1.9
26		2.5	>100	13 ± 2	
27		1.4	0.8 ± 0.2	0.13 ± 0.09	6.2
28		1.0	>100	12 ± 1	
29		3.5	21 ± 2	12 ± 3	1.8
30		2.6	22 ± 2	9.3 ± 0.3	2.4
31		2.9	9.3 ± 0.7	1.8 ± 0.2	5.2
32		2.8	15 ± 1	4.1 ± 0.7	3.7

^a NFF, neonatal foreskin fibroblasts. ^b MM96L, melanoma cells. ^c Ratio of IC₅₀s.

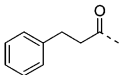
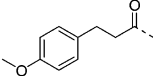
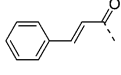
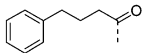
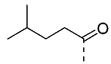
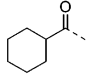
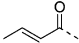
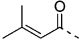
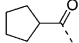
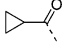
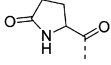
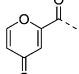
explore pharmacophore space have been useful for identifying features of this new drug class that deliver potency, much more detailed exploration of this space will be needed in our search for enhanced selectivity. In addition to further refinement of R¹ at the N-terminus of the cysteine scaffold, it is certainly conceivable that improved potency and selectivity might be obtained through alternative variations at the C- and S-termini of cysteine to achieve cytoselectivity for tumor cells over normal cells, for different types of tumor cells²⁸ and for different HDACs.

Histone Hyperacetylation. The more potent compounds from the series were tested for inhibition of histone deacetylase by monitoring the acetylation state of histone H4 using Triton–acetic acid–urea gel electrophoresis.^{29,30} Our results for this compound series are exemplified in Figure 3 for just compounds **9** and **27**, showing hyperacetylation of H4. It was not necessary to quantitate histone deacetylation because the compounds inhibit HDAC activity in both normal and cancer cells and has no impact on the cytoselectivity. The known HDAC inhibitor, TSA, included for comparison, showed similar levels of hyperacetylation indicated by

the mobility shift of histone H4. Clearly visible in untreated cells is the nonacetylated histone H4 (lane 1, arrow A). In the extracts from cells treated with 10 μg/mL of **9** and **27**, histone H4 was observed in a variety of acetylation states, ranging from nonacetylated to tetraacetylated. These results support the notion that this compound series inhibits HDACs.

Induction of p21 Expression. It has been postulated that histone acetylation is associated with activation of gene transcription.^{31,32} It has been shown^{33,34} that the action of HDAC inhibitors on gene expression is somewhat selective and does not lead to global deregulation of transcription as may be expected. In cells cultured with TSA, the expression of only 2% of genes was significantly altered, indicating a remarkable specificity. Possibly the best characterized gene to be induced following exposure to different HDAC inhibitors is that of the cyclin-dependent kinase inhibitor p21^{WAF1/Cip1}, which blocks cyclin-dependent kinase activity thereby causing cell-cycle arrest in G1.³⁵ HDAC inhibitors are thought to act directly on the *CDKN1A* promoter rather than an upstream target. The HDAC inhibitor SAHA induces accumulation of acetylated histones in the

Table 3. Structure–Activity Relationships for Analogues of **2**

Compound	R ¹	Log D _{7,0}	IC ₅₀ NFF (μM) ^a	IC ₅₀ MM96L (μM) ^b	Selectivity ^c
33		1.5	21 ± 3	7.4 ± 0.5	2.9
34		1.4	16 ± 1	8 ± 1	2.0
35		2.2	0.8 ± 0.2	0.2 ± 0.1	4.0
36		2.6	11 ± 2	5 ± 1	2.2
37		1.8	25 ± 4	7 ± 2	3.6
38		1.5	10 ± 1	5 ± 2	2.0
39		0.4	>100	11 ± 0.7	
40		0.8	22 ± 1	11 ± 1	2.0
41		1.0	>100	21 ± 3	
42		0	>100	21 ± 2	
43		0.9	9.6 ± 0.9	4.4 ± 0.3	2.2
44		-0.3	>100	>100	

^a NFF, neonatal foreskin fibroblasts. ^b MM96L, melanoma cells. ^c Ratio of IC₅₀s

Table 4. Cytotoxicity for Various Cancer Cell Lines

compound	cell line ^a IC ₅₀ (μM)							
	NFF	MM96L	SkMel	DO4	DU145	MCF7	JAM	C18013S
9	0.35 (7)	0.14 (9)	3.0 (3)	2.0 (3)	0.61 (4)	0.59 (5)	1.24 (6)	0.7 (2)
11	0.83 (9)	0.2 (1)	5.7 (4)	3.5 (2)	3.8 (4)	1.16 (2)	3.0 (2)	1.5 (3)
27	0.8 (2)	0.13 (9)	1.7 (2)	1.3 (4)	0.4 (4)	0.84 (9)	0.75 (8)	0.4 (3)
35	0.8 (2)	0.2 (1)	2.5 (1)	2.1 (3)	1.70 (3)	0.7 (2)	1.8 (1)	0.6 (5)
1a	0.20 (4)	0.03 (1)	0.28 (4)	0.09 (2)	0.06 (1)	0.02 (1)	0.08 (3)	0.06 (2)

^a NFF, neonatal foreskin fibroblasts; MM96L, SK-MEL-28 and DO4 melanoma; DU145, prostate; MCF-7, breast; JAM, CI-80-13S, ovarian. Standard deviations are in parentheses.

chromatin associated with the *CDKN1A* gene, and this correlates with the observed increase in transcription. Sp-1 transcription factor binding sites in the promoter of *CDKN1A* are considered to be crucial for the observed induction³⁴ and for a number of other targets. The capacity of novel compounds to induce expression of the cyclin-dependent kinase inhibitor p21^{WAF1/Cip1} (*CDKN1A*) was examined by semiquantitative RT-PCR after 8/24 h of treatment in MM96L and NFF cell types. Typical results on p21 expression for this compound series are shown (Figure 4) for just compound **11** tested at a concentration of 10 μg/mL against MM96L melanoma cells. Total RNA was isolated following 16 and 24 h treatment, and induction of mRNA for p21^{WAF1/Cip1} was

clearly detectable after 16 h, showing over 2-fold induction at this time consistent with observations for other HDAC inhibitors. The commercially available HDAC inhibitors, Scriptaid and Sirtinol (Calbiochem), were at least 1 order of magnitude less potent and less selective than **11** and other compounds in this series.

Morphological Reversion. Malignancy is often associated with a phenotype characterized by morphological distortion of normal cytoskeleton and cell shape. Compounds that can revert the transformed morphology of malignant cells to that of a normal phenotype may be valuable new classes of antitumor drugs.

Hydroxamic acids **9**, **11**, **27**, and **35** were found to induce dramatic changes in cellular shape in MM96L

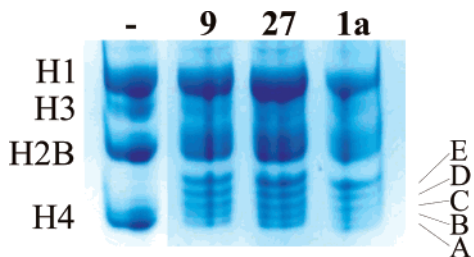


Figure 3. Acetylation of histones. MM96L cells were treated with 5 $\mu\text{g}/\text{mL}$ of test compounds for 8 h, before harvest and analysis of histone H4 acetylation by Triton-acetic acid-urea gel (Saito et al., 1991; Qiu et al., 1999). Lane 1: untreated. Lane 2: **9**. Lane 3: **27**. Lane 4: TSA. Nonacetylated (A), monoacetylated (B), diacetylated (C), triacetylated (D), and tetraacetylated (E) histone H4 are indicated.

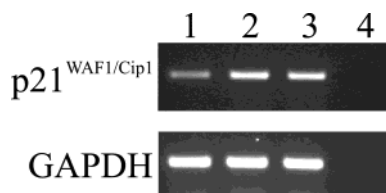


Figure 4. Induction of p21 expression. MM96L cells were treated with **11** (10 $\mu\text{g}/\text{mL}$), and total RNA was isolated from cells, reverse transcribed using SuperScript II and oligo-dT primer, and cDNA amplified by PCR using primers specific for p21^{WAF1/Cip1} and GAPDH. Lane 1, untreated; lane 2, 16 h treatment; lane 3, 24 h treatment; lane 4, RT-PCR negative control. Quantitation of p21^{WAF1/Cip1} induction was performed by densitometric analysis using ImageQuaNT 4.2 software (Molecular Dynamics, Sunnyvale, CA) following normalization to GAPDH product intensity. Expression of p21^{WAF1/Cip1} was increased 2.1-fold above that of untreated cells at both the 16 and 24 h time points.

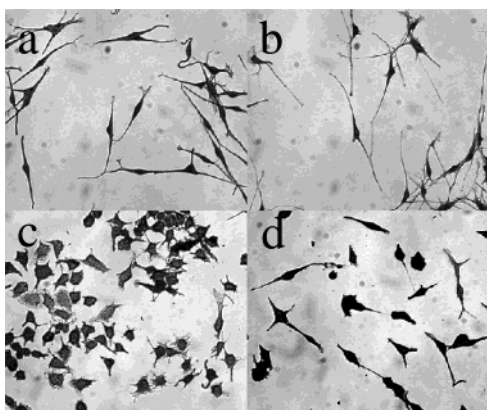


Figure 5. Morphological reversion after 24 h. (a) Untreated normal melanocytes. (b) Normal melanocytes treated with **27** (10 $\mu\text{g}/\text{mL}$). (c) Untreated melanoma cells (MM96L); (d) MM96L treated with **27** (10 $\mu\text{g}/\text{mL}$).

cells, photographed after 24 h treatment with 10 $\mu\text{g}/\text{mL}$ drug. On the other hand treatment of normal human melanocytes (or fibroblasts, data not shown) with these compounds caused no apoptosis or differentiation at doses that were toxic and differentiated tumor cell lines. Figure 5 exemplifies these effects for compound **27**, on (a) nontreated melanocytes, (b) melanocytes treated with compound **27**, 10 $\mu\text{g}/\text{mL}$ for 24 h, (c) nontreated MM96L (human melanoma cells), and (d) MM96L treated with compound **27**, 10 $\mu\text{g}/\text{mL}$ for 24 h. Clearly compound **27** profoundly alters the spherical morphology of surviving melanoma cells, making them

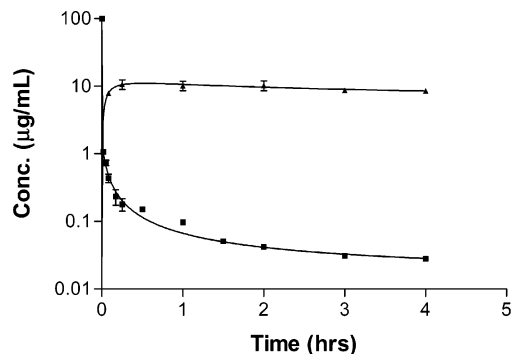


Figure 6. Oral bioavailability. Time dependent plasma concentration of **11** after oral (\blacktriangle) and intravenous (\blacksquare) administration at 5 mg/kg to each of three Wistar rats.

more dendritic like normal melanocytes which were not visibly altered by the drug(s).

Oral Bioavailability. Still the most effective form of drug delivery, in terms of ease of administration, probability of patient compliance, and systemic penetration, is the oral route which is still the preferred form of delivery of antitumor drugs. Since the most potent known HDAC inhibitors are not orally bioavailable, we thought it to be important to briefly examine one of the compounds to see whether this new series had the expected favorable properties for oral delivery. The compound series being developed here is, in general, orally bioavailable. Compound **11** (Log $D_{7.0}$ 2.7) was administered intravenously and orally to rats. When delivered at 5 mg/kg in 4:1 olive oil:DMSO to three rats starved prior to dosing, high serum levels of drug were maintained (Figure 6), with $C_{\text{max}} \sim 6 \mu\text{g}/\text{mL}$ for > 4 h examined in this preliminary study and $T_{\text{max}} \sim 15$ min. Neither vehicle nor fasting had any significant effects on these parameters.

Conclusions. Information on enzymes that regulate acetylation, transcription, and the cell cycle has increased exponentially over the past few years. HDAC enzymes have become particularly well studied and their roles in regulating transcription by mechanisms involving modification of histones as well as other proteins, while not entirely clear, are becoming better understood. HDAC inhibitors can arrest growth and induce differentiation and/or apoptotic cell death in a variety of human and normal cancer cell lines, with histones becoming hyperacetylated in both normal and tumor cells. While there is a need for new inhibitors that are selective for individual HDACs to identify their specific roles, a general HDAC inhibitor pharmacophore might be useful for evolving more tumor-selective compounds even if HDACs themselves are not the origin of cytoselective antitumor activity. Conceivably, the antiproliferative, apoptotic, and differentiating properties of HDAC inhibitors could be made more specific for tumor cells.

We have demonstrated a new series of compounds, derived simply from L-cysteine, that show potent cytotoxicity for cancer cell lines. There was some albeit limited selectivity for cancer cells (e.g. MM96L) over normal cells (e.g. NFF), although this selectivity was not maintained for the other cancer cell lines tested. The series is based on inhibiting HDAC enzymes, demonstrated through assays for hyperacetylation of histones, induction of p21 expression, and selective morphological

reversion of tumor cells. Elsewhere we have reported that HDAC inhibitors arrest a G2 phase checkpoint in normal cells but that this checkpoint is defective in tumor cells,^{27,36} and this may account for some selectivity in their cytotoxic action on tumor cells. This paper reports an early stage of our studies toward enhancing tumor-selective drug action, focusing on simple changes to the N-terminus of cysteine in an attempt to begin probing pharmacophore space corresponding to the inhibitor region most likely to interact with HDAC residues at the entrance to its active site. Further optimization at the N-, C-, and S-termini of the cysteine scaffold should provide a great deal of scope for generating compounds with greater potency and selectivity, through more effective interactions with HDACs or other cellular targets. Such enhancements are expected to make this class of compounds more effective molecular probes, not only of complex interactions with the HDAC family of enzymes, but also of other cellular targets that may be responsible for possibly separate pharmacophores for tumor cytotoxicity, cytoselectivity, and phenotypic reversion. The observed oral bioavailability augers well for further development of this class of antitumor drug.

Experimental Methods

General Methods. ¹H NMR spectra were recorded on either a Bruker ARX 500 MHz or a Varian 300 MHz NMR spectrometer. Semipreparative scale rpHPLC separations were performed on a Phenomenex Luna 5 μ C18(2) 250 \times 21 mm column run at 20 mL/min using gradient mixtures of water/0.1% TFA (A) and water:acetonitrile (90%)/0.1% TFA (B), and product fractions were always lyophilized to dryness. Preparative scale rpHPLC separations were performed on a Vydac 218TP101550 50 \times 250 mm column run at 70 mL/minute using gradient mixtures of A and B. Accurate mass determinations were performed on an API QSTAR mass spectrometer using electron impact ionization. Water-octanol partition coefficients (Log *D*) were calculated using PALLAS prolog D 2.1. Molecular modeling was performed on an SGI Octane R12000, with minimization calculation performed with the cff91 force field using the Discover Module within InsightII. Combinatorial chemistry was performed using Bohdan 48-well mini-blocks on a Bohdan 2-position vortex mixer. Resin cleavage was performed using a Bohdan vacuum collection base, and the cleavage solution was removed in a heated centrifuge chamber under vacuum.

4-Chlorobutyric Acid *tert*-Butyl Ester (45). 4-Chlorobutyl chloride (16.6 mL, 147 mmol) was added dropwise to a cooled (0 °C) solution of DMAP (10 mg) in equal portions of *tert*-butyl alcohol (50 mL) and pyridine (50 mL). After complete addition of the acid chloride, the resulting suspension was stirred for 1 h and then solvent removed under reduced pressure. The residue was dissolved in EtOAc (500 mL) and washed successively with saturated NaHCO₃ and NaCl solutions. The organic layer was dried over magnesium sulfate, and solvent was removed to provide the *tert*-butyl ester as a clear oil (22.3 g, 85%). ¹H NMR (CDCl₃, 300 MHz): 3.58 (t (6.4 Hz), 2H); 2.40 (t (7.3 Hz), 2H); 2.06 (m, 2H); 1.45 ppm (s, 9H). ¹³C NMR (CDCl₃, 75 MHz): 172.5, 81.1, 44.8, 33.1, 28.6, 28.4 ppm.

4-Iodobutyric Acid *tert*-Butyl Ester (46). Sodium iodide (70.0 g, 467 mmol) was added to *tert*-butyl ester **45** (22.0 g, 124 mmol) dissolved in THF (300 mL), and the resulting yellow suspension was refluxed overnight. The solvent was removed under reduced pressure, and the residue was dissolved in EtOAc (200 mL). After washing successively with water and saturated NaCl solution, the organic phase was dried over magnesium sulfate, and solvent was removed to provide the title iodide as a yellow oil (31.4 g, 94%). ¹H NMR (CDCl₃, 300

MHz): 3.23 (t (6.7 Hz), 2H); 2.34 (t (7.3 Hz), 2H); 2.07 (m, 2H); 1.40 ppm (s, 9H). ¹³C NMR (CDCl₃, 75 MHz): 173.2, 81.0, 44.6, 35.1, 28.9, 6.0 ppm.

4-[(2*S*)-Amino-2-carboxyethylsulfanyl]butyric Acid *tert*-Butyl Ester (3). A suspension of cysteine (6.6 g, 55.5 mmol) in methanol (50 mL) was cooled to 0 °C and degassed under a stream of argon for 5 min. On addition of 2 M sodium hydroxide solution (55.5 mL, 111 mmol) the cysteine dissolved, and *tert*-butyl ester **46** (15.0 g, 55.5 mmol) was added immediately in one portion. Stirring was continued for a further 5 min, before adjustment of the pH to ~8 with 2 M HCl. The solvent was removed under reduced pressure, and the residue desalted by rpHPLC to provide the title amino acid as a white solid (14.2 g, 97%). ¹H NMR (DMSO-*d*₆, 300 MHz): 3.4 to 3.1 (br s, water); 2.97 (dd (3.8, 14.3 Hz), 1H); 2.70 (dd (8.7, 14.2 Hz), 1H); 2.51 (t (7.4 Hz), 2H); 2.29 (t (7.2 Hz), 2H); 1.72 (m, 2H); 1.38 ppm (s, 9H). ¹³C NMR (DMSO-*d*₆, 75 MHz): 175.2, 172.6, 80.2, 53.9, 34.0, 33.2, 30.6, 28.1, 24.7 ppm.

4-[(2*S*)-Carboxy-2-(9*H*-fluoren-9-ylmethoxycarbonylamino)ethylsulfanyl]butyric Acid *tert*-Butyl Ester (47). NaHCO₃ (14 g, 170 mmol) and Fmoc-OSu (18.7 g, 55.5 mmol) were added to a solution of amino acid **3** (14.0 g, 53.0 mmol) dissolved in 1:1 THF-water (300 mL), and the resulting solution was stirred for 2 h. The solvent was removed under reduced pressure, and the residue was suspended in EtOAc (300 mL) and washed successively with water, 1 M HCl, saturated NaHCO₃ solution, and brine. The organic layer was dried over magnesium sulfate, and solvent was removed under reduced pressure to yield a yellow oil which was purified by rpHPLC to provide the title acid as a white solid (19.7 g, 76%). ¹H NMR (DMSO-*d*₆, 300 MHz): 7.90 (d (7.5 Hz), 2H); 7.73 (d (7.71 Hz), 2H); 7.42 (t (7.2 Hz), 2H); 7.32 (t (6.6 Hz), 2H); 4.65 (d (5.3 Hz), 2H); 4.30 (m, 2H); 2.91 (dd (3.7, 14.2 Hz), 1H); 2.76 (dd (8.6, 14.2 Hz), 1H); 2.51 (t (7.3 Hz), 2H); 2.26 (t (7.2 Hz), 2H); 1.72 (m, 2H); 1.39 ppm (s, 9H). ¹³C NMR (DMSO-*d*₆, 75 MHz): 174.6, 172.1, 156.2, 144.2, 144.1, 128.0, 127.4, 125.6, 120.5, 79.6, 60.5, 54.5, 46.8, 34.0, 33.2, 30.8, 28.1, 24.8 ppm.

4-[(2*S*)-Allyloxycarbonyl-2-(9*H*-fluoren-9-ylmethoxycarbonylamino)ethylsulfanyl]butyric Acid *tert*-Butyl Ester (4). Allyl bromide (6.23 g, 51.5 mmol) was added in one portion to a suspension of K₂CO₃ (27 g, 200 mmol) and acid **47** (25.0 g, 51.5 mmol) in DMF (200 mL). The resulting solution stirred for 10 min, and then the solvent was removed under reduced pressure. The resulting residue was dissolved in EtOAc (500 mL) and washed successively with water, 1 M HCl, saturated NaHCO₃ solution, and brine. The organic layer was dried over magnesium sulfate, and solvent was removed under reduced pressure to provide the title allyl ester as a yellow oil (25.0 g, 92%). ¹H NMR (DMSO-*d*₆, 300 MHz): 7.89 (d (7.60 Hz), 2H); 7.72 (d (7.71 Hz), 2H); 7.41 (t (7.1 Hz), 2H); 7.32 (t (7.3 Hz), 2H); 5.88 (m, 1H); 5.31 (d (16.7 Hz), 1H); 5.20 (d (11.7 Hz), 1H); 4.59 (d (5.3 Hz), 2H); 4.25 (m, 4H); 2.88 (dd (3.8, 14.1 Hz), 1H); 2.77 (m, 1H); 2.53 (t (7.3 Hz), 2H); 2.27 (t (7.3 Hz), 2H); 1.72 (m, 2H); 1.38 ppm (s, 9H). ¹³C NMR (DMSO-*d*₆, 75 MHz): 172.1, 170.9, 156.3, 144.1, 141.1, 132.6, 128.0, 127.4, 125.6, 120.5, 118.1, 80.0, 66.2, 60.1, 54.5, 47.0, 34.0, 32.7, 31.0, 28.1, 24.9 ppm.

4-[2-Allyloxycarbonyl-2-(9*H*-fluoren-9-ylmethoxycarbonylamino)ethylsulfanyl]butyric Acid (48). *tert*-Butyl ester **4** (25.0 g, 47.5 mmol) was stirred in 99:1 TFA:water (50 mL) for 2 h. The solvent was removed under reduced pressure, and the residue was purified by rpHPLC to provide the title acid as a white solid (19.5 g, 88%). ¹H NMR (DMSO-*d*₆, 300 MHz): 7.89 (d (7.1 Hz), 2H); 7.72 (d (7.1 Hz), 2H); 7.42 (t (7.1 Hz), 2H); 7.33 (t (7.6 Hz), 2H); 5.90 (m, 1H); 5.30 (d (17.3 Hz), 1H); 5.19 (d (9.4 Hz), 1H); 4.59 (d (5.2 Hz), 2H); 4.28 (m, 4H); 2.89 (dd (4.9, 13.5 Hz), 1H); 2.79 (m, 1H); 2.52 (t (7.3 Hz), 2H); 2.29 (t (7.3 Hz), 2H); 1.73 ppm (m, 2H). ¹³C NMR (DMSO-*d*₆, 75 MHz): 174.4, 170.9, 156.3, 144.1, 141.1, 132.6, 128.0, 127.4, 125.6, 120.5, 118.4, 66.2, 60.1, 54.5, 47.0, 32.8, 32.7, 31.1, 24.7 ppm.

Coupling of Acid 48 to Resin. Commercially available N-Fmoc hydroxylamine 2-chlorotriyl resin (0.77 mmol/g, 10 g, 7.7 mmol) was shaken gently with 1:1 piperidine:DMF (30

mL) overnight and then flow washed with DMF for 1 min. In a separate flask, HATU (3.0 g, 7.8 mmol) was added to a solution of acid **48** (3.7 g, 7.8 mmol) and DIPEA (5.3 mL, 31.2 mmol) dissolved in DMF (10 mL), and the resulting solution was stirred gently for 5 min. The HATU activated acid was then added in one portion to the deprotected resin, and the resin was shaken gently for 1 h. After washing the resin well with DMF, the resin loading was determined to be 0.46 mmol/g (70%) (LRMS *m/e* calcd for C₂₅H₂₉N₂O₆S (MH⁺) 485.6, obsd 485.1). The unreacted resin was then acylated by addition of a solution of acetic anhydride (842 mg, 7.8 mmol) and DIPEA (5.3 mL, 31.2 mmol) in DMF (20 mL) with shaking for 2 min, followed by thorough washing with DMF.

Removal of the Allyl Ester. The resin was flow washed with DCM for 2 min and then shaken in DCM (30 mL) for a further 10 min. An argon stream was introduced, and the resin and DCM were degassed for 5 min. DMBA (1.2 g, 7.9 mmol) was added, and bubbling was continued for a further minute to ensure thorough mixing. Pd(Ph₃)₄ (270 mg, 0.23 mmol) was added to the resin, the flask was wrapped in aluminum foil, and after a further 30 s of degassing the argon stream was removed and the resin shaken gently for 1 h. The resin was flow washed successively with DCM, DMF, and DCM, before drying under high vacuum. (The resin loading was determined to be 0.45 mmol/g (LRMS *m/e* calcd for C₂₂H₂₅N₂O₆S (MH⁺) 445.5, obsd 445.2).

Coupling of Benzylamine. The resin (0.45 mmol/g, 200 mg, 0.09 mmol) was shaken in DMF (1 mL) for 10 min, and then DIPEA (122 μ L, 0.72 mmol) and 0.5 M HBTU in DMF (360 μ L, 0.18 mmol) were introduced and shaking continued for a further 5 min. Benzylamine (0.25 mmol) was then added, and shaking was continued for a further 1 h. After the resin is washed well with DMF, cleavage of a small portion of resin and analysis by mass spectroscopy generally indicates 60–85% conversion to the amide. Repeating the coupling provides complete conversion.

Coupling of Acids (General Procedure). The resin was shaken in DMF (1 mL) for 10 min, the DMF removed, and then 1:1 piperidine:DMF (1 mL) added. After being shaken for 5 min, the piperidine:DMF was removed, and the resin was washed well with DMF. This procedure was repeated two more times. In a separate flask 0.5 M HBTU (180 μ L, 90 μ mol) in DMF was added to a solution of the desired acid (90 μ M) and DIPEA (76 μ L, 450 μ mol) in DMF (1 mL), and the resulting solution was stirred for 5 min before being added in one portion to the resin. The resin was shaken for 1 h and then washed well with DMF. Cleavage of a small portion of resin and analysis by mass spectroscopy generally indicates 100% conversion to the amide.

Cleavage of the Product from the Resin (General Procedure). The resin was washed well with DCM and then drained. TFA:water (99:1, 1 mL) was added, and the resin was shaken for 20 min. The TFA was collected, and the resin was washed with a further 1 mL of TFA. The TFA was removed by distillation. Purification was performed by rpHPLC, and hydroxamates were confirmed to be greater than 95% pure by analytical rpHPLC and ¹H NMR spectroscopy. All hydroxamic acids displayed high field ¹H NMR spectral and HRMS parameters consistent with their proposed structures. Representative examples are given below.

Hydroxamic acid 9 (R¹ = 4-dimethylaminobenzoic acid): ¹H NMR (DMSO-*d*₆, 500 MHz): 10.32 (s, 1H); 10.02 (s, 1H); 8.51 (t (5.9 Hz), 1H); 8.14 (d (8.3 Hz), 1H); 7.70 (d (8.7 Hz), 2H); 7.24 to 7.10 (m, 5H); 6.63 (d (8.7 Hz), 2H); 4.52 (m, 1H); 4.21 (d (5.9 Hz), 2H); 2.89 (s, 6H); 2.86 (obs m (5.2 Hz)); 2.76 (dd (9.5, 13.5 Hz), 1H); 2.44 (m, 2H); 1.94 (t (7.5 Hz), 2H); 1.64 ppm (m, 2H). HRMS calcd for C₂₃H₃₁N₄O₄S (MH⁺): 459.206, Found 459.201.

Hydroxamic acid 11 (R¹ = 4-bromobenzoic acid): ¹H NMR (DMSO-*d*₆, 500 MHz): 10.27 (s, 1H); 8.63 (d (7.9 Hz), 1H); 8.56 (t (5.5 Hz), 1H); 7.76 (d (8.7 Hz), 2H); 7.61 (d, 7.9 Hz), 2H); 7.25 to 7.15 (m, 5H); 4.54 (m, 1H); 4.21 (d (5.5 Hz), 2H); 2.90 (dd (4.8, 13.5 Hz), 1H); 2.75 (dd (9.5, 13.5 Hz), 1H);

2.45 (m, 2H); 1.93 (br t (7.1 Hz), 2H); 1.65 ppm (m, 2H). HRMS calcd for C₂₁H₂₅BrN₃O₄S (MH⁺): 494.074, Found 494.076.

Hydroxamic acid 25 (R¹ = 2-naphthoic acid): ¹H NMR (DMSO-*d*₆, 500 MHz): 10.30 (s, 1H); 10.04 (s, 1H); 8.70 (d (7.9 Hz), 1H); 8.60 (t (6.3 Hz), 1H); 8.45 (s, 1H); 7.97 to 7.87 (m, 4H); 7.52 (m, 2H); 7.25 to 7.10 (m, 5H); 4.63 (m, 1H); 4.25 (d (5.5 Hz), 2H); 2.95 (dd (4.8, 13.5 Hz), 1H); 2.83 (ddd (1.6, 9.5, 13.5 Hz), 1H); 2.49 (m, 2H); 1.96 (m, 2H); 1.67 ppm (m, 2H). HRMS calcd for C₂₅H₂₈N₃O₄S (MH⁺): 466.179, Found 466.178.

Hydroxamic acid 27 (R¹ = 1H-indole-2-carboxylic acid): ¹H NMR (DMSO-*d*₆, 500 MHz): 11.52 (s, 1H); 10.28 (s, 1H); 8.61 (t (6.0 Hz), 1H); 8.53 (d (8.3 Hz), 1H); 7.55 (d (7.9 Hz), 1H); 7.34 (d (7.9 Hz), 1H); 7.25 to 7.20 (m, 6H); 7.10 (t (7.1 Hz), 1H); 6.96 (t (7.1 Hz), 1H); 4.60 (m, 1H); 4.24 (m, 2H); 2.91 (dd (5.5, 13.9 Hz), 1H); 2.77 (dd (9.5, 13.9 Hz), 1H); 2.47 (m, 2H); 1.95 (br t (6.7 Hz), 2H); 1.66 ppm (m, 2H). HRMS calcd for C₂₃H₂₇N₄O₄S (MH⁺): 455.175, Found 455.171.

Hydroxamic acid 35 (R¹ = cinnamic acid): ¹H NMR (DMSO-*d*₆, 500 MHz): 10.29 (s, 1H); 8.62 (t (5.5 Hz), 1H); 8.32 (d (7.9 Hz), 1H); 7.47 (br d (7.13 Hz), 2H); 7.37 to 7.10 (m, 9H); 6.71 (d (15.9 Hz), 1H); 4.52 (dd (7.9, 14.2 Hz), 1H); 4.22 (d (6.3 Hz), 2H); 2.80 (dd (6.3, 13.5 Hz), 1H); 2.65 (dd (7.9, 13.5 Hz), 1H); 2.45 (t (7.1 Hz), 2H); 1.96 (br t (7.9 Hz), 2H); 1.65 ppm (m, 2H). HRMS calcd for C₂₃H₂₈N₃O₄S (MH⁺): 442.179, Found 442.176.

Cell Lines and Culture Medium. All cell lines used have been described previously^{37,38} and were cultured in 10% heat-inactivated foetal calf serum (CSL, Australia) in RPMI 1640 medium supplemented with 100 U/mL penicillin, 100 μ g/mL streptomycin, and 3 mM HEPES at 5% CO₂, 99% humidity at 37 °C. Primary human melanocytes and fibroblasts were obtained from neonatal foreskins and cultured in the above medium, with addition of 1 mM pyruvate, 0.2 mM nicotinamide, 6 ng/mL cholera toxin, and 16.2 nM TPA (Sigma, St. Louis, MO) in the case of melanocytes. Melanocytes were cultured at 5% CO₂/5% O₂/90% N₂ with 99% humidity at 37 °C as described.³⁹ Routine mycoplasma tests were performed using Hoechst stain⁴⁰ and were always negative.

Cell Survival. Clonogenic cell survival was determined by fixing cells grown and treated in microtiter plates, followed by staining with acidic sulforhodamine (SRB). This has the advantages of sensitivity (fluorescence detection), ability to perform immunohistochemistry subsequently on the fixed cells and being amenable to automation and high throughput analysis. Treatments were generally at minimally toxic doses (10–50% clonogenic survival).

Cells were plated into 96-well microtiter plates at 5 × 10³ cells/well and allowed to adhere overnight. Compounds were added to culture medium at the indicated concentrations, and plates were incubated in the above conditions for 24 h. Following this incubation period, compounds and media were removed and replaced with fresh culture medium. Cells were then grown for a further 72 h before assay using sulforhodamine B (SRB; Sigma, St. Louis, MO) as previously described.^{41,42} Briefly, the culture medium was removed from the 96-well microtiter plates, and the plates were washed twice with phosphate-buffered saline (PBS), before the cells were fixed with methylated spirits for 15 min. The plates were then rinsed with tap water and the fixed cells stained with 50 μ L/well of SRB solution (0.4% sulforhodamine B (w/v) in 1% (v/v) acetic acid) over a period of 1 h. The SRB solution was then removed from the wells, and the plates were rapidly washed two times with 1% (v/v) acetic acid. Protein bound dye was then solubilized by addition of 100 μ L of 10 mM unbuffered Tris and incubated for 15 min at 25 °C. Plates were then read at 564 nm on a VERSA max tuneable microplate reader (Molecular Devices, Sunnyvale, CA).

Histone Hyperacetylation. Analysis of histone H4 acetylation by Triton-acetic acid-urea gel was carried out as previously described.²⁷

Cell Treatment and Total RNA Isolation. Cells were seeded in 25 cm² flasks in 10% heat-inactivated foetal calf serum (CSL, Melbourne, Australia) in RPMI 1640 medium supplemented with 100 U/mL penicillin, 100 μ g/mL strepto-

mycin, 3 mM HEPES, and incubated at 5% CO₂, 99% humidity at 37 °C for 16 h before treatment. Cells were treated with 10 µg/mL of drug and RNA harvested at the indicated times following treatment. Total RNA was extracted from cells using the Qiagen RNeasy Kit as per manufacturer's instructions. RNA was analyzed for sufficient quality by formamide agarose gel electrophoresis and quantified by spectrophotometry.

p21 Expression. The semiquantitative analysis of mRNA expression of p21^{WAF1/Cip1} was carried out by RT-PCR. First strand synthesis was performed using 2 µg of total RNA with 0.5 µg of oligo (dT)₁₅ and 200 U SuperScript II (Invitrogen, Carlsbad, CA), at 42 °C for 50 min in a final volume of 20 µL. Polymerase chain reaction was performed using 10 µL of a 1 in 10 dilution of the first strand cDNA, under standard conditions with the polymerase DyNAzyme (Finnzymes, Melbourne, Australia). Oligonucleotide primers and conditions used in the PCR were as follows: p21^{WAF1/Cip1} F 5'-ATT AGC AGC GGA ACA AGG AGT CAG ACA T-3', p21^{WAF1/Cip1} R 5'-CTG TGA AAG ACA CAG AAC AGT ACA GGG T-3' with initial denaturation at 94 °C for 7 min, 27 cycles of 94 °C for 45 s, 60 °C for 40 s and 72 °C for 60 s, with the final extension for 5 min; GAPDH F 5'-GGC TCT CCA GAA CAT CAT CCC TGC-3', GAPDH R 5'-GGG TGT CGC TGT TGA AGT CAG AGG-3' with initial denaturation at 94 °C for 7 min, 25 cycles of 94 °C for 45 s, 62 °C for 40 s and 72 °C for 60 s, with the final extension for 5 min. Products were analyzed by agarose gel electrophoresis and visualized on a UV light box. Product intensity was determined to increase linearly with number of cycles and amount of mRNA used, by densitometric analysis using ImageQuant 4.2 software (Molecular Dynamics, Sunnyvale, CA). Quantitation of p21^{WAF1/Cip1} induction was also performed by densitometric analysis using ImageQuant 4.2 software following normalization to GAPDH product intensity.

Morphological Reversion. Cells were plated into 96-well microtiter plates at 5 × 10³ cells/well and allowed to adhere overnight. Compounds were added to culture medium at the indicated concentrations and plates incubated in the above conditions for 24 h. Cells were then washed once with Hank's Balanced Salt Solution (HBSS; Gibco/Invitrogen, Grand Island, NY), and fixed in 4% buffered formalin for 1 h at room temperature. The fixed cells were then washed once further with HBSS and stained with 1% Crystal Violet in methanol for 5 min. Excess stain was removed by washing with tap water, before the microtiter plate being air-dried at 37 °C. Photographs were taken using a Leica DMIRB inverted microscope.

Acknowledgment. We thank the Australian Research Council and The Hans Werthén Foundation for fellowship support to D.F. and P.K. and NHMRC for support to P.P.

Appendix

Abbreviations. Ac = acetyl; DCM = dichloromethane; DIPEA = diisopropylamine; DMAP = 4-(dimethylamino)pyridine; DMBA = 1,3-dimethylbarbituric acid; DMF = dimethylformamide; EtOAc = ethyl acetate; Fmoc-OSu = 9-fluorenylmethoxycarbonyl-*N*-hydroxysuccinimide; HATU = *O*-(7-azabenzotriazol-1-yl)-1,1,3,3-tetramethyluronium hexafluorophosphate; HBTU = [(benzotriazolyl)oxy]-*N,N,N,N*-tetramethyluronium hexafluorophosphate; rpHPLC = reverse phase high performance liquid chromatography; LRMS = low resolution mass spectroscopy; TFA = trifluoroacetic acid; THF = tetrahydrofuran; TSA = trichostatin A.

Supporting Information Available: Mass spectral and HPLC data. This material is available free of charge via the Internet at <http://pubs.acs.org>.

References

- Marks, P. A.; Richon, V. M.; Kiyokawa, H.; Rifkind, R. A. Induced differentiation of transformed cells with hybrid polar compounds: a cell cycle-dependent process. *Proc. Natl. Acad. Sci. U.S.A.* **1994**, *91*, 10251–10254.
- Rifkind, R. A.; Richon, V. M.; Marks, P. A. Induced differentiation, the cell cycle and the treatment of cancer. *Pharmacol. Ther.* **1996**, *69*, 97–102.
- Leszczyniecka, M.; Roberts, T.; Dent, P.; Grant, S.; Fisher, P. B. Differentiation therapy of human cancer: basic science and clinical implications. *Pharmacol. Ther.* **2001**, *90*, 105–156.
- Vigushin, D. M.; Coombes, R. C. Histone deacetylase inhibitors in cancer treatment. *Anti-Cancer Drugs* **2002**, *13*, 1–13.
- Marks, P. A.; Rifkind, R. A.; Richon, V. M.; Breslow, R.; Miller, T.; Kelly, W. K. Histone deacetylases and cancer: causes and therapies. *Nature* **2001**, *1*, 194–202.
- Richon, V. M.; Emiliani, S.; Verdin, S.; Webb, Y.; Breslow, R.; Rifkind, R. A.; Marks, P. A. A class of hybrid polar inducers of transformed cell differentiation inhibits histone deacetylases. *Proc. Natl. Acad. Sci. U.S.A.* **1998**, *95*, 3003–3007.
- Parsons, P. G.; Hansen, C.; Fairlie, D. P.; West, M. L.; Danoy, P. A. C.; Sturm, R. A.; Dunn, I. S.; Pedley, J.; Ablett, E. M. Tumor Selectivity and Transcriptional Activation by Azalaic Bishydroxamic Acid in Human Melanocytic Cells. *Biochem. Pharmacol.* **1997**, *53*, 1719–1724.
- Su, G. H.; Sohn, T. A.; Ryu, B.; Kern, S. E. A Novel Histone Deacetylase Inhibitor Identified by High-Throughput Transcriptional Screening of a Compound Library. *Cancer Res.* **2000**, *60*, 3137–3142.
- Butler, L. M.; Agus, D. B.; Sher, H. I.; Higgins, B.; Rose, A.; Cordon-Cardo, C.; Thaler, H. T.; Rifkind, R. A.; Marks, P. A.; Richon, V. M. Suberoylanilide Hydroxamic Acid, an inhibitor of Histone Deacetylase, Suppresses the Growth of Prostate Cancer Cells in Vitro and in Vivo. *Cancer Res.* **2000**, *60*, 5165–5170.
- Tsuji, N.; Kobayashi, M.; Nagashima, K.; Wakisaka, Y.; Koizumi, K. A new antifungal antibiotic, trichostatin. *J. Antibiot.* **1976**, *29*, 1–6.
- Yoshida, M.; Kijima, M.; Akita, M.; Beppu, T. Potent and specific inhibition of mammalian histone deacetylase both in vivo and in vitro by trichostatin A. *J. Biol. Chem.* **1990**, *265*, 17174–17179.
- Kijima, M.; Yoshida, M.; Sugita, K.; Horinouchi, S.; Beppu, T. Trapoxin, an antitumor cyclic tetrapeptide, is an irreversible inhibitor of mammalian histone deacetylase. *J. Biol. Chem.* **1993**, *268*, 22429–22435.
- Darkin-Rattray, S. J.; Gurnett, A. M.; Myers, R. W.; Dulski, P. M.; Crumley, T. M.; Allocco, J. J.; Cannova, C.; Meinke, P. T.; Colletti, S. L.; et al. Apicidin: a novel antiprotozoal agent that inhibits parasite histone deacetylase. *Proc. Nat. Acad. Sci. U.S.A.* **1996**, *93*, 13143–13147.
- Yoshida, M.; Furumai, R.; Nishiyama, M.; Komatsu, Y.; Nishino, N.; Horinouchi, S. Histone deacetylase as a new target for cancer chemotherapy. *Cancer Chemother. Pharmacol.* **2001**, *48*, S20–S26.
- Furumai, R.; Komatsu, Y.; Nishino, N.; Khochbin, S.; Yoshida, M.; Horinouchi, S. Potent histone deacetylase inhibitors built from trichostatin A and cyclic tetrapeptide antibiotics including trapoxin. *Proc. Nat. Acad. Sci. U.S.A.* **2001**, *98*, 87–92.
- Murray, P. J.; Kranz, M.; Ladlow, M.; Taylor, S.; Berst, F.; Holmes, A. B.; Keavey, K. N.; Jaxa-Chamiec, A.; Seale, P. W.; Stead, P.; Upton, R. J.; Croft, S. L.; Clegg, W.; Elsegood, M. R. J. The synthesis of cyclic tetrapeptide analogues of the antiprotozoal natural product apicidin. *Bioorg. Med. Chem. Lett.* **2001**, *11*, 773–776.
- Taunton, J.; Collins, J. L.; Schreiber, S. L. Synthesis of Natural and Modified Trapoxins, Useful Reagents for Exploring Histone Deacetylase Function. *J. Am. Chem. Soc.* **1996**, *118*, 10412–10422.
- Komatsu, Y.; Tomizaki, K.; Tsukamoto, M.; Kato, T.; Nishino, N.; Sato, S.; Yamori, T.; Tsuuro, T.; Furumai, R.; Yoshida, M.; Horinouchi, S.; Hayashi, H. Cyclic hydroxamic-acid-containing peptide 31, a potent synthetic histone deacetylase inhibitor with antitumor activity. *Cancer Res.* **2001**, *61*, 4459–4460.
- Cairns, B. R. Emerging roles for chromatin remodelling in cancer biology. *Trends Cell Biol.* **2001**, *11*, S15–S21.
- Cress, W. D.; Seto, E. Histone deacetylase, transcriptional control, and cancer. *J. Cell. Physiol.* **2000**, *184*, 1–16.
- Schlake, T.; Klehr-Wirth, D.; Yoshida, M.; Beppu, T.; Bode, J. Gene expression within a chromatin domain: the role of core histone hyperacetylation. *Biochemistry* **1994**, *33*, 4197–4206.
- Marks, P. A.; Richon, V. M.; Breslow, R.; Rifkind, R. A. Histone deacetylase inhibitors as new cancer drugs. *Curr. Opin. Oncol.* **2001**, *13*, 477–483.
- Grozinger, C. M.; Schreiber, S. L. Deacetylase enzymes: Biological functions and the use of small-molecule inhibitors. *Chem. Biol.* **2002**, *9*, 3–16.

- (24) Johnstone, R. W. Histone-deacetylase inhibitors: Novel drugs for the treatment of cancer. *Nature Rev.* **2002**, *1*, 287–299.
- (25) Finnin, M. S.; Donigian, J. R.; Cohen, A.; Richon, V. M.; Rifkind, R. A.; Marks, P. A.; Breslow, R.; Pavletich, N. P.; Structures of a histone deacetylase homologue bound to the TSA and SAHA inhibitors. *Nature* **1999**, *401*, 188–193.
- (26) Marmorstein, R. Structure of Histone Deacetylases: Insights into Substrate Recognition and Catalysis. *Structure* **2001**, *9*, 1127–1133.
- (27) Qiu, L.; Burgess, A.; Fairlie, D. P.; Leonard, H.; Parsons, P. G.; Gabrielli, B. G. Histone deacetylase inhibitors trigger a G2 checkpoint in normal cells that is defective in tumor cells. *Mol. Biol. Cell.* **2000**, *11*, 2069–2083.
- (28) Krämer, O. H.; Göttlicher, M.; Heinzl, T. Histone deacetylase as a therapeutic target. *Trends Endocrinol. Metab.* **2001**, *12*, 294–300.
- (29) Saito, S.; Crissman, H. A.; Nishijima, M.; Kagabu, T.; Nishiya, I.; Cram, L. S. Flow cytometric and biochemical analysis of dose-dependent effects of sodium butyrate on human endometrial adenocarcinoma cells. *Cytometry* **1991**, *12*, 757–764.
- (30) Qiu, L.; Kelso, M. J.; Hansen, C.; West, M. L.; Fairlie, D. P.; Parsons, P. G. Anti-tumour activity in vitro and in vivo of selective differentiating agents containing hydroxamate. *Br. J. Cancer* **1999**, *80*, 1252–1258.
- (31) Marks, P. A.; Richon, V. M.; Breslow, R.; Rifkind, R. A. Histone deacetylase inhibitors as new cancer drugs. *Curr. Opin. Oncol.* **2001**, *13*, 477–483.
- (32) Gregory, P. D.; Wagner, K.; Horz, W. Histone acetylation and chromatin remodeling. *Exp. Cell. Res.* **2001**, *265*, 195–202.
- (33) Van-Lint, C.; Emiliani, S.; Verdin, E. Expression of a small fraction of cellular genes is changed in response to histone acetylation. *Gene Express.* **1996**, *5*, 245–253.
- (34) Richon, V. M.; Sandhoff, T. W.; Rifkind, R. A.; Marks, P. A. Histone deacetylase inhibitor selectively induces p21WAF1 expression and gene-associated histone acetylation. *Proc. Natl. Acad. Sci. U.S.A.* **2000**, *97*, 10014–10019.
- (35) Burgess, A. J.; Pavey, S.; Warrener, R.; Hunter, L. K.; Piva, T. J.; Musgrove, E. A.; Saunders, N.; Parsons, P. G.; Gabrielli, B. G. Up-regulation of p21^{WAF1/CIP1} by Histone Deacetylase Inhibitors Reduces Their Cytotoxicity. *Mol. Pharmacol.* **2001**, *60*, 1–10.
- (36) Warrener, R.; Beamish, H.; Burgess, A.; Waterhouse, N. J.; Giles, N.; Fairlie, D. P.; Gabrielli, B. Tumour cell-selective cytotoxicity by targeting cell cycle checkpoints. *FASEB J.* **2003**, *17*, 1550–1552.
- (37) Parsons, P. G.; Bowman, E. P. W.; Blakely, R. L. Selective toxicity of deoxyadenosine analogues in human melanoma cell lines. *Biochem. Pharmacol.* **1986**, *35*, 4025–4029.
- (38) Todaro, G. J.; Fryling, C.; De Larco, J. E. Transforming growth factors produced by certain human tumour cells: polypeptides that interact with epidermal growth factor receptors. *Proc. Natl. Acad. Sci. U.S.A.* **1980**, *77*, 5258–5262.
- (39) Xu, C.; Parsons, P. G. Cell cycle delay, mitochondrial stress and uptake of hydrophobic cations induced by sunscreens in cultured human cells. *Photochem. Photobiol.* **1999**, *69*, 611–616.
- (40) Chen, T. R. In situ detection of mycoplasma contamination in cell cultures by fluorescent Hoechst 33258 stain. *Exp. Cell. Res.* **1977**, *104*, 255–262.
- (41) Skehan, P.; Storeng, R.; Scudiero, D.; Monks, A.; McMahon, J.; Vistica, D.; Warren, J. T.; Bokesch, H.; Kenney, S.; Boyd, M. R. New colorimetric cytotoxicity assay for anticancer-drug screening. *J. Natl. Cancer Inst.* **1990**, *82*, 1107–1112.
- (42) Rubinstein, L. V.; Shoemaker, R. H.; Paull, K. D.; Simon, R. M.; Tosini, S.; Skehan, P.; Scudiero, D. A.; Monks, A.; Boyd, M. R. Comparison of in vitro anticancer-drug-screening data generated with a tetrazolium assay versus a protein assay against a diverse panel of human tumor cell lines. *J. Natl. Cancer Inst.* **1990**, *82*, 1113–1118.

JM030222I